Silicon (2022) 14:11395–11403
https://doi.org/10.1007/s12633-022-01871-9

ORIGINAL PAPER

Growth Mechanism and Kinetics of Siliconizing of AISI D2 Tool Steel

Mojtaba Najafizadeh[1] · Morteza Hosseinzadeh[2] · Mehran Ghasempour-Mouziraji[3,4] · Mansoor Bozorg[5] · Angelo Perrone[6] · Pasquale Cavaliere[6]

Received: 11 February 2022 / Accepted: 2 April 2022 / Published online: 11 April 2022

Abstract
The present paper goes into details of the kinetics of silicide layer growth on AISI D2 during surface siliconizing. Pack cementation was employed in order to siliconize the steel surface. Siliconizing was conducted by using powder mixtures Si 12 wt.% + NH_4Cl 0.5 wt.% + Al_2O_3 at 923, 1073 and 1223 K for 2 to 6 h, respectively. Thermodynamic calculations showed that growth mechanisms of the coating comprise many different chemical reactions. The microstructure and silicides precipitation evolution were analyzed through scanning electron microscopy (SEM), energy dispersive X-ray spectroscopy (EDS), X-ray diffraction analysis (XRD). The silicides layers thickness falls in the range 32–154 μm. The coatings hardness varied between 750 and 800 HV, being dependent on the process parameters. The kinetics measurement revealed the growth of the FeSi, Fe_2Si and $FeSi_2$ sub-layers as a function of treatment time and temperature. The results illustrated that the diffusion coefficient (k) increased with the treatment temperature. Activation energy (Q) was calculated as 788.83 $kJ.mol^{-1}$. The crystal growth rate resistance (K) ranged from 5.2×10^{-9} to 3.1×10^{-8} $cm^2.s^{-1}$.

Keywords Coating · Siliconizing · Kinetics · Diffusion · Activation energy

1 Introduction

The wide forming applications of AISI D-type steels is due to the exceptional retention of strength properties at elevated temperatures [1–4]. Anyway, the change of wear resistance from an abrasive to an adhesive character as the hardness is increased leads to serious issues regarding the fracture behavior due to excessive brittleness especially at the service temperatures [5, 6]. For this reason, it is necessary to develop hard and stable coatings to be employed in the protection of these tool steels surfaces in order to provide a barrier to the cracks initiation during long term forming operations. In this way it is possible to provide high surface hardness without modifying the bulk ductility of the steel components. Among the available coatings technologies, pack cementation is demonstrated to provide very useful modifications of AISI D2 surfaces by improving the in service life [7]. In this direction,

✉ Mansoor Bozorg
bozorg.mansoor@gmail.com

✉ Pasquale Cavaliere
pasquale.cavaliere@unisalento.it

Mojtaba Najafizadeh
mojtaba@sjtu.edu.cn

Morteza Hosseinzadeh
m_hosseinzadeh59@yahoo.com

Mehran Ghasempour-Mouziraji
mehran@ua.pt

Angelo Perrone
angelo.perrone@unisalento.it

[1] The State Key Laboratory of Metal Matrix Composites, School of Materials Science and Engineering, Shanghai Jiao Tong University, Shanghai 200240, China

[2] Department of Engineering, Islamic Azad University of Ayatolah Amoli, Amol, Iran

[3] EMaRT Group, School of Design, Management and Production Technologies, University of Aveiro, Estrada do Cercal 449, 3720-509 Oliveira de Azeméis, Portugal

[4] TEMA - Centre for Mechanical Technology and Automation, University of Aveiro, Aveiro, Portugal

[5] Department of Chemical and Materials Engineering, Shahrood University of Technology, Shahrood 3619995161, Iran

[6] Department of Innovation Engineering, University of Salento, Via per Arnesano, 73100 Lecce, Italy

Halide Activated Pack Cementation (HAPC) has been largely optimized for many complex and hard alloys [8, 9]. In this process, the cementation powders react at high temperature with the steel surface in a very active and efficient way thanks to the vapors formation activated by the halide compounds. As usual in the diffusion processes, the temperature level provides the driving force for the active elements penetration as well as for the hardening compounds precipitation. The optimization of the processing procedure as well as the optimization of the powders compositions allow for the obtaining of thick and stable hardening layers able to provide the mechanical strength of the treated surfaces for a very wide steel series [10]. As a matter of fact, HAPC silicide coatings can be employed for the coatings deposition on many alloy compositions [11–14]. The most active hardening solution is the formation of iron-silicon intermetallic compounds capable of producing a very hard and stable siliconized protective layer [15]. In comparison with other surface treatments largely employed for the steel protection, pack cementation is characterized by a very simple processing route, by shorter processing times and by cost savings also for massive and very complex geometries [16–19]. Obviously, depending on the volumes to be treated, on the required layers thickness as well as on the industrial times, processing parameters need to be optimized in order to obtain sound components in reasonable industrial times [20–23]. In this way, pack siliconized steel components are able to provide improved superficial mechanical properties, with an optimal retention of the bulk ductility accompanied with improved high temperature oxidation resistance and high temperature wear strength. Now, It is crucial to precisely control the hardening compounds formation and precipitation in order to obtain a very uniform precipitates distribution along the coatings layers especially in the direction of the adhesion optimization of the coating to the substrate. To do this, it is fundamental to precisely define the kinetics of the formation and precipitation processes as a function of the selected and fixed processing parameters especially in terms of the employed temperatures and treating times. In this way, exceptional surface properties can be induced in the treated steel in a very narrow window of processing parameters [24]. In the present paper, the growth kinetics of the whole pack siliconizing process were precisely defined for the cementation of AISI D2 steel in order to control the precipitation process finalized to the hardening of the surface. The growth kinetics of the compounds layers was defined by controlling the thickness and the composition of the layers, as well as the intermetallics distribution along the coatings thickness as a function of the treatment time within the temperature range 923–1223 K.

2 Experimental Procedure

2.1 Test Materials and Siliconizing

The employed bulk material was a commercial AISI D2 steel whose composition was measured by employing mass spectrometry. The steel composition was: C-1.43; Si-0.198; Mn-0.308; P-0.012; S-0.0075; Cr-12; Mo-0.8; Ni-0.0304; Cu-0.0901; V-0.124; Fe-bal (wt.%).

For the pack siliconizing treatment, cylindrical steel samples with dimensions of 30X30 mm were prepared. The steel surfaces were polished with traditional metallographic operations. Then, the cylinders were cleaned for the optimal surface preparation for the siliconizing coating procedure. The pack siliconizing finalized to the silicides hardening precipitation was performed by following the general procedure already described in a previous work from the authors [25]. The schematic of reactions during siliconizing is shown in Fig. 1. The powders employed for siliconizing were Si 12 wt.%, NH_4Cl as a halide activator with a percentage of 0.5 wt.%. Si is the main source; NH_4Cl and Al_2O_3 were employed as a chemical activator and as inert filler, respectively. The pack siliconizing was performed into ceramic cubic boxes with the dimensions of 10cx10cx10cm. The boxes were firstly filled (up to 50% of the box volume) with the cementation powders. Then, three cylinders were positioned on the powders and the boxes were finally fulfilled with the remaining cementation powders. For the diffusion process, the boxes are heated in a laboratory furnace in air atmosphere (Hefei Kejing Material Technology Company, model KSL-1400X) The processing window was set at 2 to 6 h with temperatures falling in the range 923–1223 K.

2.2 Silicide Layers Formation and Properties

The microstructure of the cross-section of the siliconized samples was examined by scanning electron microscope (SEM) observations performed through employing a *ZEISS* EVO 40 instrument equipped with energy dispersive spectroscope (EDS) in backscatter scanning electron set-up at 20 kV. The thickness of the silicides formed on the steel samples was measured from polished cross section by the SEM micrometer. The coatings phases evolution was analyzed through X-Ray diffraction with a *Rigaku* diffractometer by applying Cu-Kα radiation at an accelerating voltage of 40 kV and a current of 40 mA with a scan step of 0.02. The micro-hardness measurements of the siliconized steel were performed by using a digital Vickers micro-hardness instrument. The kinetics of layers growth was analyzed by evaluating the thickness of the silicide layers as a function of treatment time and temperature. The thermodynamic equilibrium for the coating formation reactions was analyzed by employing the HSC chemistry software version 6.

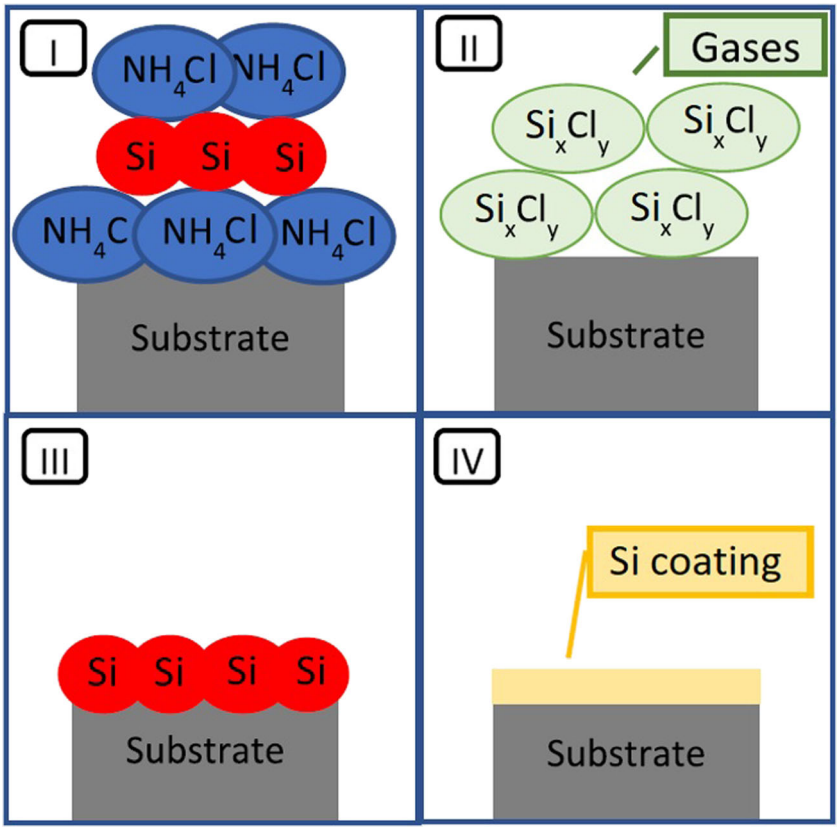

Fig. 1 Schematic of the reactions taking place during siliconizing

3 Results and Discussion

3.1 HAPC Process Model

The growth of the coating during the HAPC process was analysed by maintaining the chemical potential gradient (CPG) sufficient for the diffusion of the halide vapors close to the matrix. The chloride activator (NH_4Cl) reacted with Si by creating multiple gaseous chlorides. This is the primary stage of halogenation reaction. The NH_4Cl activator decomposes into NH_3 and HCl at a temperature close to 600 K. The large volumes of chloride and chloro-hydride vapors of $SiCl_x$ (x = 1, 2, 3, 4) and SiH_xCl_y (x = 1, 2 & y = 1, 2, 3) form depending on the reaction between HCl and Si. The chemical reactions taking place during HAPC for the NH_4Cl as activator and Si as main source can be described as follows (Eqs. 1–10) [25, 26]:

$$NH_4Cl_{(s)} \rightarrow NH_{3(g)} + HCl_{(g)} \quad (1)$$

$$2NH_{3_{(g)}} \rightarrow N_{2_{(g)}} + 3H_{2_{(g)}} \quad (2)$$

$$4HCl_{(g)} + Si_{(l)} \rightarrow SiCl_{4_{(g)}} + 4H \quad (3)$$

On the substrate:

$$3SiCl_{4_{(g)}} + Si_{(s)} \rightarrow 4SiCl_{3_{(g)}} \quad (4)$$

$$2SiCl_{3_{(g)}} + Si_{(s)} \rightarrow 3SiCl_{2_{(g)}} \quad (5)$$

$$SiCl_{2_{(g)}} + Si_{(s)} \rightarrow 2SiCl_{(g)} \quad (6)$$

$$H_{(g)} + Cl_{(g)} \rightarrow HCl_{(g)} \quad (7)$$

$$Si + Cl_2 + H_2 \rightarrow SiH_2Cl_2 \quad (8)$$

$$Si + \left(\frac{3}{2}\right)Cl_2 + \left(\frac{1}{2}\right)H_2 \rightarrow SiHCl_3 \quad (9)$$

$$Fe + Si \rightarrow FeSi, FeSi_2 \text{ or } Fe_2Si \quad (10)$$

The deposition of the silicon on the surface of the substrate developed by the silicon chloride and silicon chloro-hydride gas phases. This was driven by the CPG by assuming that the silicon close to the substrate surface is completely used. The migrating of the chloride vapor can be calculated by Fick's first law Eq. (11) [27]:

$$J_i = \left(\frac{D_i}{RT}\right)\frac{\Delta P_i}{\Delta x} \quad (11)$$

Where J_i is the flux of the chloride vapor, D_i is the inter-diffusion coefficient of gas phase, R is the ideal gas content ($R = 8.314\ ^{J}/_{K.mol}$), T is the absolute temperature, ΔP_i is the change of the nominal pressure for each specie 'i' that is fixed as the nominal pressure of each component in the embedded powder ($\alpha_{si} = 1$) minus the nominal pressure of the specie in

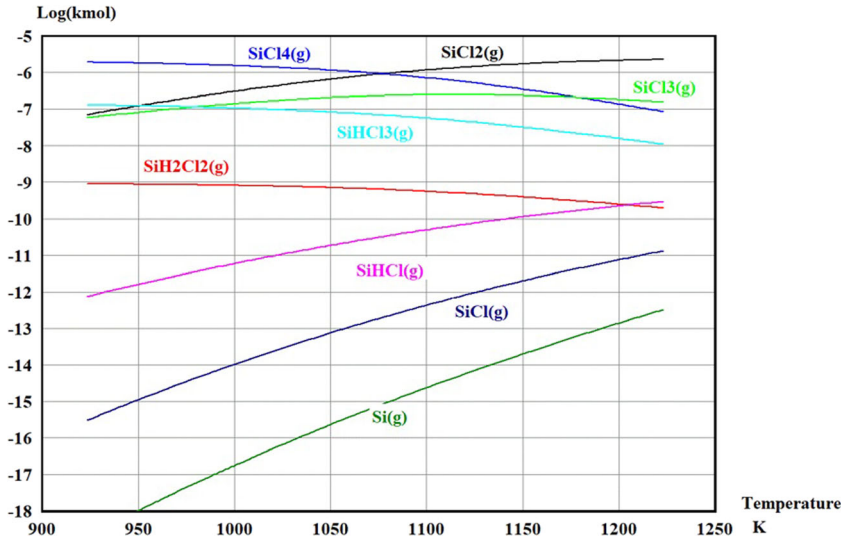

Fig. 2 Partial Pressure of the main chloride and hydro chloride vs. temperature during HAPC process

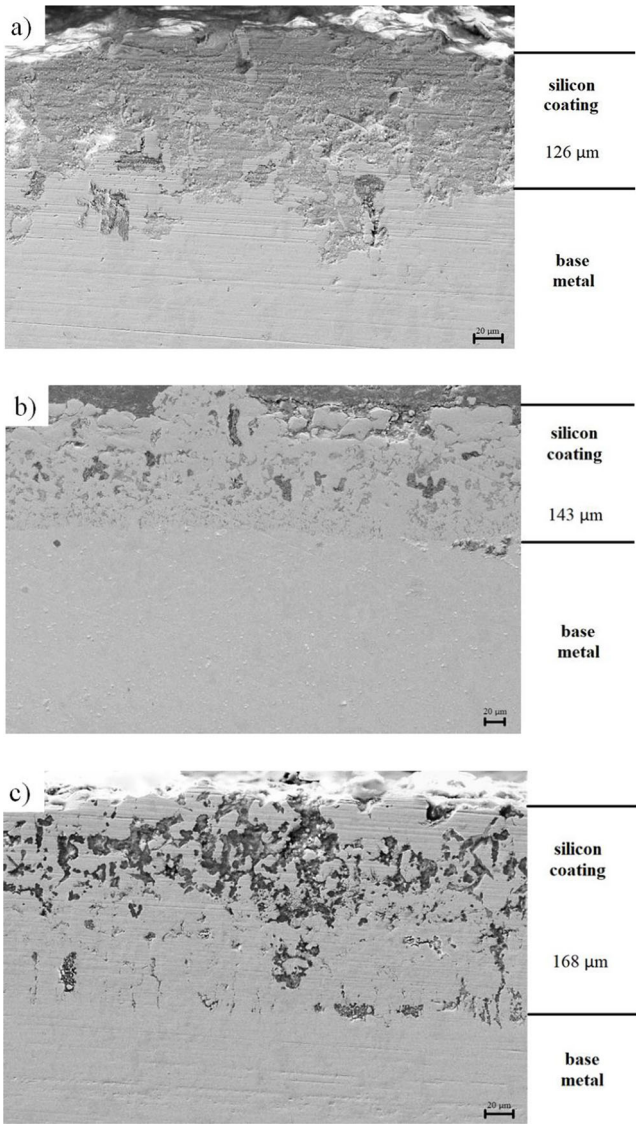

Fig. 3 SEM microstructure of siliconized AISI D2 tool steel at 1223 K for (**a**) 2 h, (**b**) 3 h, (**c**) 4 h, (**d**) 5 h and (**e**) 6 h

the matrix, and Δx is the width of the reduction zone. The vapor migration to the substrate surface and the coating formation has direct effect on the change of nominal pressure ΔP_i of $SiCl_x$ (x = 1, 2, 3, 4) and SiH_xCl_y (x = 1, 2 & y = 1, 2, 3) vapors [28–30].

First of all it was supposed that the chloride $SiCl_x$ (x = 4) and hydro chloride SiH_xCl_y (x = 2 & y = 2, 3) were completely used during the process. The concentration of the chloride and hydro chloride hardly provided enough chlorine or hydro chlorine to support deposition [34]. Due to the total internal pressure in the pack approaching the

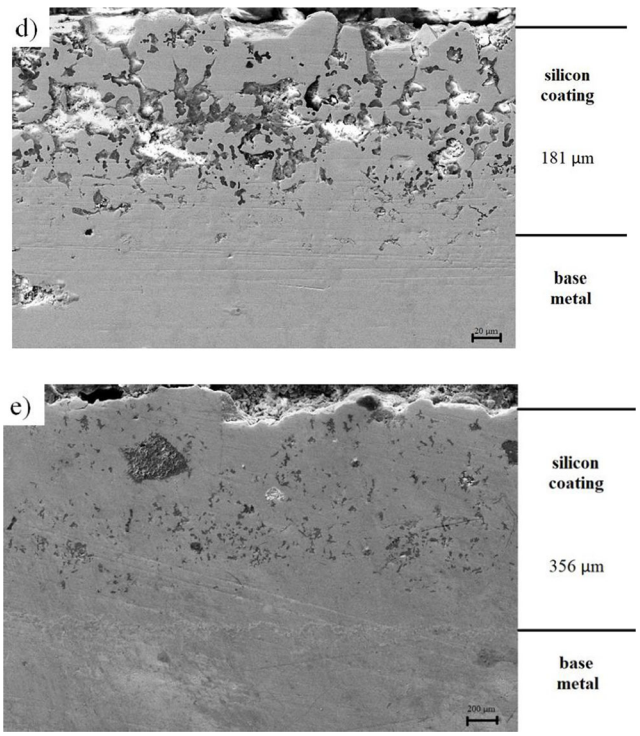

Fig. 3 continued.

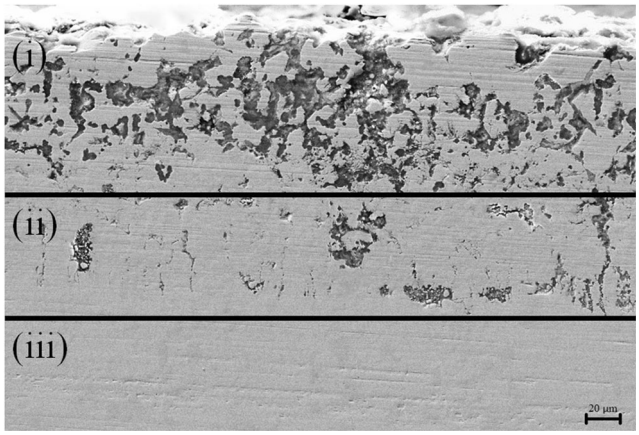

Fig. 4 SEM image of the siliconizing coating on the AISI D2 tool steel at 1223 K for 4 h

atmosphere one and due to the retained mass balance, the equilibrium partial pressure for the various chlorides in the mixture including 12 wt% Si, 0.5 wt% NH_4Cl, and 87.5 wt% Al_2O_3 at the different temperatures has been calculated and showed in Fig. 2. Among all these chlorides and hydro chlorides, the partial pressures of $SiCl_2$ and $SiHCl_3$ were the largest in the considered temperature range (900-1250 K). Moreover, the $SiCl_4$ and $SiCl_3$ were stable as compared to the SiCl, SiHCl and SiH_2Cl_2 with the low vapor pressure. Hence, the deposition of the coating in HAPC was largely determined by the migration and decomposition of $SiCl_2$ and $SiHCl_3$.

3.2 Properties of the Silicide Layers

The cross-section aspect of the siliconized AISI D2 tool steel examined with the SEM is shown in Fig. 3. The formed silicide layers are highlighted in the picture with the indication of

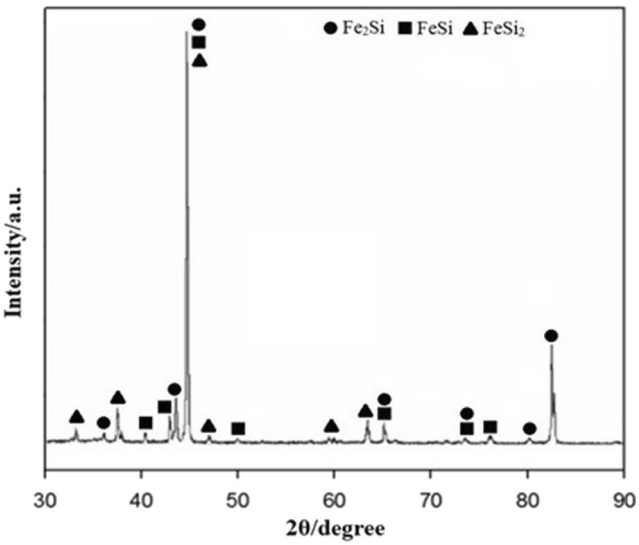

Fig. 5 XRD pattern of the silicide coating formed on the AISI D2 tool steel by the pack cementation method at 1223 K for 4 h

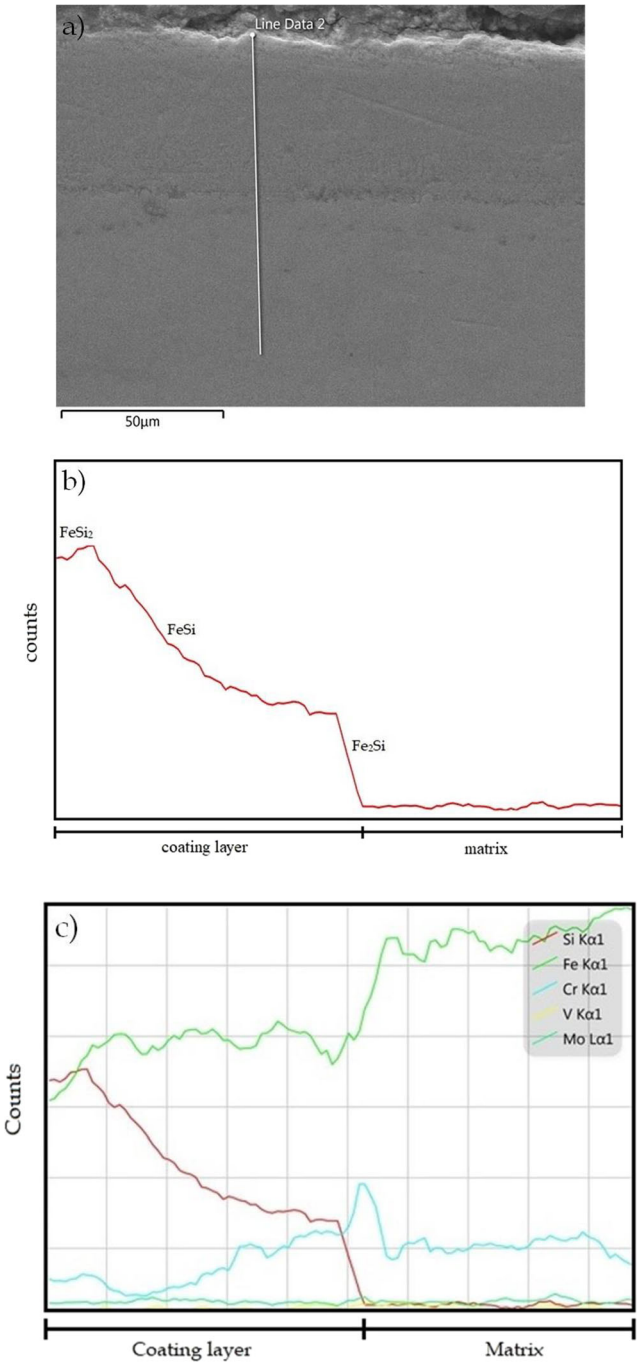

Fig. 6 **a** SEM micrograph, **b** and **c** EDX line scan analysis of a siliconized AISI D2 tool steel at 923 K for 3 h

the thickness. The Fig. 3a-e refers to the process conducted at the temperature of 1223 K for 2, 3, 4, 5 and 6 h respectively. The structure of the silicide layers is smooth. A rough interface is located between the base-metal and the silicide layer due to the anisotropic diffusion process, as shows in Fig. 3e. The SEM backscatter electron images showed that silicide coating had two different layers namely the inner layer (white) and the outer layer (dark), the same results was shown by Najafizadeh et al. [31] and Ugur et al. [32].

In each condition, they can be observed three different regions revealed at higher magnification (Fig. 4). They are the structures from coating to substrate zone: (i) porous structure, (ii) dense coating layer, and (iii) base-metal, the same and different structure was showed by Najafizadeh et al. [25].

The XRD analysis of the surface of the coating revealed three main phases: $FeSi_2$, FeSi, and Fe_2Si, as shown in Fig. 5. The concentration peak of the FeSi phase is higher than the $FeSi_2$ and Fe_2Si ones [30].

The EDS line analysis confirms that the silicide concentration increases from the top surface of the coating toward the substrate (Fig. 6). Also, it is valuable to nothing that, the thickness concentration of the $FeSi_2$ and Fe_2Si is lower than the FeSi phase as shown in Fig. 6b. The intensity of the iron in the Fig. 6c showed changes from interfaces between matrix/Fe_2Si phase and $Fe_2Si/FeSi_2$ phase. $FeSi_2$ and FeSi phases contain less Fe than the Fe_2Si phase. Chromium concentrated in the Fe_2Si layer selectively as shows in Fig. 6c. The continuous coating can form, when the silicon potential of the environment is higher, even less reactive points on the surface of the base-metal are involved in the process. The layer thickness is related to the boron diffusion from $FeSi_2/Fe_2Si$. There are three regions that can be recognized: (i) the surface layer, containing the $FeSi_2$, FeSi, and Fe_2Si phases, (ii) the transmission zone being rich in silicon, (iii) the matrix, which is not affected by silicon [33].

The concentration of the small diameter atoms in SEM backscatter shows darker zone than the substrate [35]. The concentrations of the silicon atoms in the outer layer of the silicide coating are higher than the inner part as shown in EDS line scan results. This indicates XRD pattern as a $FeSi_2$ phase, in the outer layer of the silicide layer. Also, the EDS line scan shows the three different phases similar to the XRD pattern. The concentration of the iron near to the base plate is obviously the highest.

Figure 7 shows the microhardness profile along the thickness from the coating surface toward the substrate. The average micro-hardness of silicide coating (770 HV) is higher than

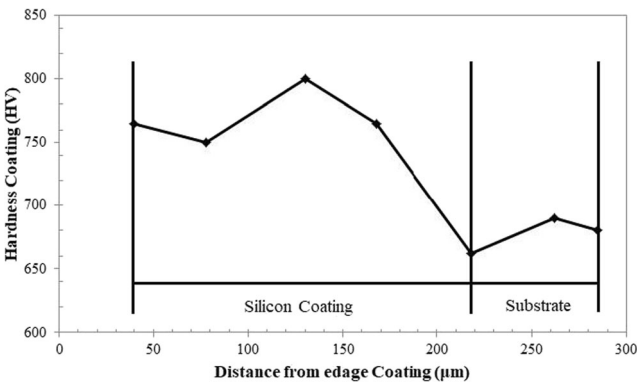

Fig. 7 Micro-hardness profile of the silicide layer formed on the siliconized AISI D2 tool steel sample at 1223 K for 4 h

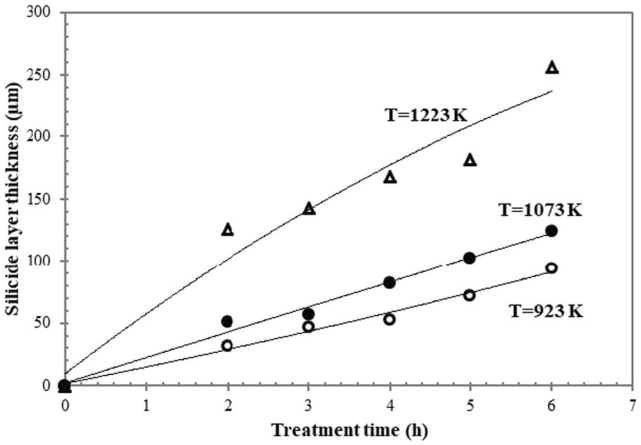

Fig. 8 Silicide layer thickness formed on AISI D2 tool steel as a function of treatment time and temperature

the steel matrix (677 HV). This is attributed to formation of the Fe-Si intermetallic compounds. The middle FeSi phase in the silicide coating was found to be harder than the other phases [33]. With increasing the treatment time and temperature the thickness of the FeSi increased in comparison to the other phases.

3.3 Silicide Layer Growth Kinetics

The thickness of the silicide layers depends on the siliconizing temperature and time. The revealed thickness ranges from 32 to 256 µm. Another factor influencing the silicide layer behavior is the substrate composition governing the diffusion kinetics of the hardening elements [36]. During the pack cementation treatments such as siliconizing, chromizing, aluminizing, the chemical compositions of the pack have effect on the thickness of the hardening layer. In Fig. 8 it is clear that there is a nearly parabolic correlation between the silicide coating thickness and the treatment time [37].

By supposing that: (i) it is possible the control of the growing rate of the silicon on the surface by diffusion of the silicon in the $FeSi_2$, FeSi and Fe_2Si and (ii) the growing of the silicide layer happens as result of direct silicon diffusion into the

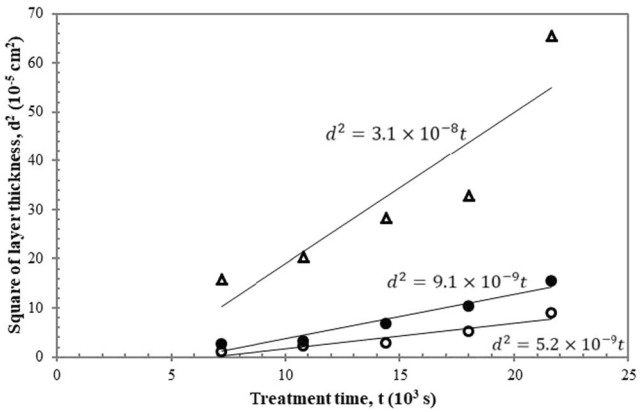

Fig. 9 Square of layer thickness (d^2) as a function of the treatment time (t)

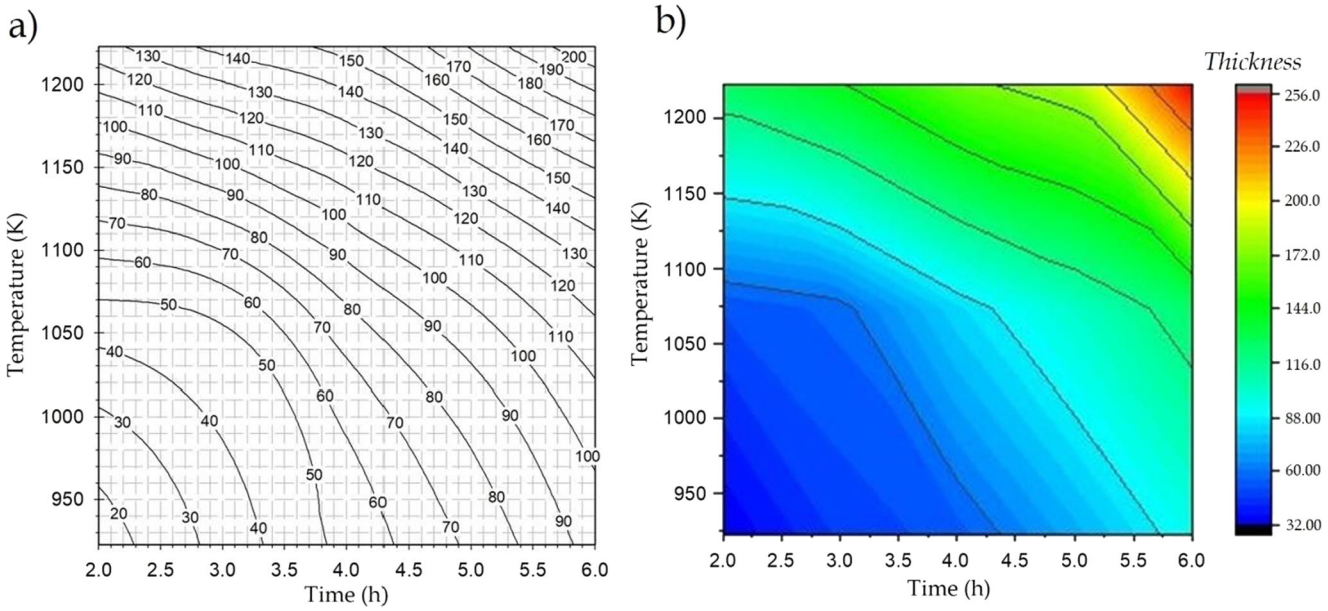

Fig. 10 Contour diagram of silicide layer thickness of siliconizing AISI D2 tool steel

surface of the substrate [38]; the different thickness of the silicide layer with time follows the parabolic law (Eq. 12):

$$d^2 = K.t \tag{12}$$

Where "d" is the thickness of the silicide layer (μm), "t" is the time of the treatment process (min) and "K" is growth rate of the silicide layer. The primary factor which plays a key role on the growth of the layer is the silicon diffusion in the silicide layer, as shown in Fig. 9.

The silicide coating fabricated at higher treatment time and temperature tends to become thicker. Moreover, a contour diagram drawn from Fig. 8 for processing parameters by employing the *Siqmaplot 12* and *Origin Pro 8* software in industrial applications can be obtained. From the contour diagram, the layer thickness can be determined for a given time and temperature as show in Fig. 10a. The results are in good agreement with the experimental observations. As shown in Fig. 10b by increasing treatment time and temperature the reaction between the powder composition inside the pack occurred easier, by supporting the increase in thickness of the coating.

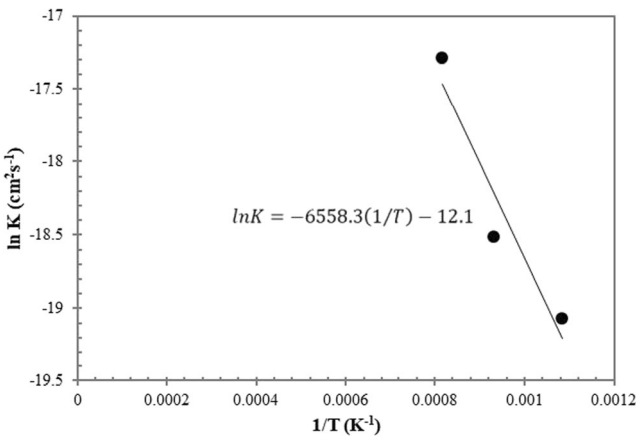

Fig. 11 ln K to 1/T for siliconized steel

The correlation between the activation energy (Q), growth rate constant (K), and the process temperature in Kelvin (T), can be described by an Arrhenius-type relationship (Eq. 13):

$$K = K_0 \exp(-Q/RT) \tag{13}$$

Where R = 8.314 is the gas constant and K_0 is the frequency factor [39]. Taking the common logarithm of Eqs. (13) and 14 is obtained:

$$\ln K = \ln K_0 + (-Q/RT) \tag{14}$$

The spot of ln "K" contra mutual treatment temperature is linear as shown in Fig. 9. It can be defined "Q" from the slope of the direct line as shows in Fig. 11.

With the increasing of the treatment temperature, the growth rate constant (K) increases, as shown in the experimental results. The activation energy (Q) was calculated for the present study, and this was determined as 788.83 KJ.mol^{-1}. The range of the growth rate constant (K) resulted in the range 5.2 × 10^{-9} to 3.1 × 10^{-8} cm^2.s^{-1}. The Eq. (15) is a formula between the growth rate constant (K) and mutual treatment temperature (1/T).

$$K = 5.56 \times 10^{-6} \exp(6558.3/T) \tag{15}$$

Where "T "and "K" stand for treatment temperature and growth rate constant, respectively. From the Eqs. (12) and (15), the coating thickness can be calculated for predetermined time and treatment temperature (Eq. 16):

$$d_{(\mu m)} = \sqrt{t \times 5.56 \times 10^{-6} \exp(6558.3/T)} \quad (16)$$

Sen et al. [32] reported that the activation energy of silicon in the silicide layer was 540 KJ.mol^{-1} and the growth rate constant by pack cementation at 1323 K, 1373 K and 1423 for 2, 4 and 6 h were between 7.76 × 10^{-7} to 2.45 × 10^{-5} mm^2.s^{-1}, respectively. The kinetic results in this study were compared with those by Yang et al. [40], the growth rate constant of silicon at 1073 K is 3.85 × 10^{-10} mm^2.s^{-1} and the activation energy was 242 KJ.mol^{-1}.

4 Conclusions

The growth kinetics of the silicide coating on the AISI D2 tool steel made by pack cementation method was investigated. The coatings thickness was evaluated as a function of the treatment time within the temperature range 923–1223 K. The main conclusions are summarized as follows:

1. The silicide layers fabricated on tool steel by the pack siliconizing are compact and have good adhesion. The silicide layers have a smooth morphology.
2. The XRD patterns of the silicide layers revealed the formation of Fe_2Si, FeSi and Fe_2Si phases. Based on the temperature and treatment time, the average hardness of the silicide layer is 700 HV. The FeSi is the phase most influencing the hardness increase of the coatings.
3. The EDS line scan of the silicide layer allowed for the precise identification of the thickness of the three phases.
4. By using contour chart, the thickness is estimated based on the temperature and treatment time. Moreover, this chart would be highly beneficial as the kinetic definition of the process related to the process parameters.
5. The growth rate constant (K) changes from 5.2 × 10^{-9} to 3.1 × 10^{-8} cm^2.s^{-1} and the activation energy for the growth of silicide layer was found to be 788.83 KJ.mol^{-1}.
6. In order to estimate hardness and thickness of the coated layer for industrial applications, temperature and time must be controlled in the best way. Based on the achieved results (contour diagram), it can be inferred that the result would be applicable for industrial and academic purposes.

Acknowledgements Not applicable.

Author Contribution All authors contributed to the study conception and design and writing. All authors read and approved the final manuscript.

Funding Open access funding provided by Università del Salento within the CRUI-CARE Agreement. The authors declare that no funds, grants, or other support were received during the preparation of this manuscript.

Data Availability Data available on request from the authors.

Declarations

Ethics Approval Not applicable.

Consent to Participate Not applicable.

Consent for Publication Not applicable.

Competing Interests The authors have no relevant financial or non-financial interests to disclose.

References

1. Kumar A, Kaur M, Singh S, Joseph A, Jhala G, Bhandari S (2018) High-temperature tribological studies of plasma-nitrided tool steels. Surf Eng 34(8):620–633
2. Gobbi SJ, Gobbi VJ, Reinke G, Muterlle PV, Rosa DM (2019) Ultra low temperature process effects on micro-scale abrasion of tool steel AISI D2. Mater Sci Technol 35(11):1355–1364
3. Khan AM, Jamil M, Ul Haq A, Hussain S, Meng L, He N (2019) Sustainable machining. Modeling and optimization of temperature and surface roughness in the milling of AISI D2 steel. Ind Lubr Tribol 71(2):267–277
4. BombačD TM, Kugler G, Peruš I (2018) Amelioration of surface cracking during hot rolling of AISI D2 tool steel. Mater Sci Technol 34(14):1723–1736
5. Yapici A, Aydin SE, Koc V, Kanca E, Yildiz M (2019) Wear behavior of Borided AISI D2 steel under linear reciprocating sliding conditions. Prot Met Phys Chem Surf 55(2):341–351
6. Sadeghi B, Shamanian M, Ashrafizadeh F, Cavaliere P, Rizzo A (2018) Wear behavior of Al-based nanocomposites reinforced with bimodal micro- and Nano-sized Al2O3 particles produced by spark plasma sintering. Mater Perf Charact 7(1):327–350
7. Keddam M, Kulka M (2018) Simulation of the growth kinetics of FeB and Fe2B layers on AISI D2 steel by the integral method. Phys Met Metallogr 119(9):842–851
8. Xiang J, Xie F, Wu X, Yu Y (2019) Microstructure and tribological properties of Si-Y/Al two-step deposition coating prepared on Ti2AlNb based alloy by halide activated pack cementation technique. Tribol Int 136:45–57
9. Tian J, Yu WH, Tian W, Zhao J, Li YQ, Liu YZ (2015) Effects of Y-Ce on wear behaviours of silicide coatings. Surf Eng 31(4):289–294
10. Lu XJ, Xiang ZD (2017) A novel single-step surface-treatment process for forming Cr-nitride coatings on steels. Metall Mater Trans A48:580–583

11. Sun J, Li T, Zhang G-P, Fu Q-G (2019) Different oxidation protection mechanisms of HAPC silicide coating on niobium alloy over a large temperature range. J Alloys Compd 790:1014–1022
12. Byeong WL (2018) Effect of diffusion coatings on the high temperature properties of nickel-chromium-superalloys. Int J Mod Phys B 32:1840056
13. Chaia N, Portebois L, Mathieu S, David N, Vilasi M (2017) On the interdiffusion in multilayered silicide coatings for the vanadiumbased alloy V-4Cr-4Ti. J Nucl Mater 484:148–156
14. Li X, Hu G, Tian J, Tian W, Xie W, Li X (2018) Wear resistance enhancement of Ti-6Al-4V alloy by applying Zr-modified silicide coatings. J Mater Eng Perform 27:1073–1082
15. Xue J, Tao G, Tang C, Xu N, Li F, Yin C (2020) Effect of siliconizing with molten salt on the wear resistance and corrosion resistance of AISI 302 stainless steel. Surf Coat Technol 382: 125217
16. Semboshi S, Kimura S, Iwase A, Ohtsu N (2014) Surface hardening of age-hardenable cu–Ti dilute alloys by plasma nitriding. Surf Coat Technol 258:691–698
17. Ikeda J, Semboshi S, Iwase A, Gao W, Sugawara A (2015) Precipitation behavior and properties of cu-Ti alloys with added nitrogen. Mater Trans 56(3):297–302
18. Ueyama D, Semboshi S, Saitoh Y, Ishikawa N, Nishida K, Soneda N, Hori F, Iwase A (2014) Hardening induced by energetic electron beam for Cu–Ti alloys. Japan J Appl Phys 53(5S1):05FC04
19. Perepezko JH, Sossaman TA, Taylor M (2017) Environmentally resistant Mo-Si-B-based coatings. J Therm Spray Technol 26(5): 929–940
20. Cockeram BV, Rapp RA (1995) The kinetics of multilayered titanium-silicide coatings grown by the pack cementation method. Met Trans A26:777–791
21. Qiao Y, Zheng K, Guo X (2019) Microstructure formation of silicide coating on Nb–W–Mo–Zr alloy. Surf Eng 35(7):588–595
22. Shao W, Cui Y, Zhou C (2019) Diffusion paths of silicide coatings on Nb-Si-based alloys during pack cementation process. Metall Mater Trans A50(6):2945–2955
23. Xiang ZD, Datta PK (2003) Codeposition of Al and Si on nickel base superalloys by pack cementation process. Mater Sci Eng A356:136–144
24. Genel K, Ozbek I, Bindal C (2003) Kinetics of boriding of AISI W1 steel. Mater Sci Eng A357:311–314
25. Najafizadeh M, Ghasempour-Mouziraji M, Sadeghi B, Cavaliere P (2021) Characterization of Tribological and mechanical properties of the Si3N4 coating fabricated by duplex surface treatment of pack siliconizing and plasma Nitriding on AISI D2 tool steel. Metall Mater Trans A52(11):4753–4766
26. Chakraborty SP, Banerjee S, Sharma IG, Suri AK (2010) Development of silicide coating over molybdenum based refractory alloy and its characterization. J Nucl Mater 403:152–159
27. Wang C, Li K, He Q, Huo C, Shi X (2018) Oxidation and ablation resistant properties of pack-siliconized Si-C protective coating for carbon/carbon composites. J Alloys Compd 741:937–950
28. Xue Q, Sun CY, Yu JY, Huang L, Wei J, Zhang J (2017) Microstructure evolution of a Zn-Al coating co-deposited on low-carbon steel by pack cementation. J Alloys Compd 699:1012–1021
29. Tarani E, Stathokostopoulos D, Tsipas SA, Chrissafis K, Vourlias G (2021) Effect of the deposition time and heating temperature on the structure of chromium Silicides synthesized by pack cementation process. Corros Mater Degrad 2(2):210–226
30. Najafizadeh M, Ghasempour-Mouziraji M (2021) Multi-objective optimization of process parameters in pack siliconizing on AISI D2 steel. Silicon 13(7):2233–2242
31. Najafizadeh M, Hosseinzadeh M, Ghasempour-Mouziraji M, Perrone A, Cavaliere P (2022) Pack siliconizing optimization of AISI D2 tool steel. Silicon:1–11
32. Ugur S, Azkan O, Senol Y, Saduman S (2013) Kinetics of iron silicide deposited on AISI D2 steel by pack method. Proceedings of the 22nd international conference on metallurgy and materials. Czech Republic, Brno, pp 15–17
33. Najafizadeh M, Ghasempour-Mouziraji M, Zhang D (2021) Silicon diffusion in silicide coatings deposition by the pack cementation method on AISI D2 tool steel. Silicon:1–8
34. Chaiaa N, Cury PL, Rodrigues G, Coelho GC, Nunes CA (2020) Aluminide and silicide diffusion coatings by pack cementation for Nb–Ti–Al alloy. Surf Coat Technol 389:125675
35. Sen S, Sen U, Bindal C (2005) The growth kinetics of borides formed on boronized AISI 4140 steel. Vacuum 77:195–202
36. Yener T (2019) Low temperature aluminising of Fe-Cr-Ni super alloy by pack cementation. Vacuum 162:114–120
37. Pierre D, Peronnet M, Bosselet F, Viala JC, Bouix J (2002) Chemical interaction between mild steel and liquid mg-Si alloys. Mater Sci Eng B94:186–195
38. Gas P, d'Heurle FM (1993) Formation of silicide thin films by solid state reaction. Appl Surf Sci 73:153–161
39. Yang Y, Zhang F, He J, Qin Y, Liu B, Yang M, Yin F (2018) Microstructure, growth kinetics and mechanical properties of interface. Vacuum 151:189–196
40. Yang HL, Cui CW, Li YG, Tang GZ, Zhang YZ (2011) Growth kinetics and microstructure of siliconized layer by molten salt electrodeposition. Adv Mater Res 214:434–438